

Conceptual Demonstration of Hydrogen Peroxide Based Electrochemical Propulsion with Rotating Gliding Arc

Jeongrak Lee,* Seonghyeon Kim,† and Anna Lee‡
Pohang University of Science and Technology (POSTECH), Pohang 376-73, Republic of Korea and

Ju Won Kim[§] and Hongjae Kang[¶]

Korea Institute of Machinery and Materials, Daejeon 341-03, Republic of Korea

https://doi.org/10.2514/1.J064284

The development of high-performance green monopropellant-based small thrusters is essential for successful multipurpose space missions. This study experimentally demonstrates a novel electrochemical propulsion system that leverages rotating gliding arc (RGA) plasma to enhance the performance of 88 wt% hydrogen peroxide. This is the first electrochemical propulsion system that utilizes catalytic decomposition gases of hydrogen peroxide directly as plasma-forming gases and an alternating current (AC)-based RGA. The system employs an AC power supply operating at a 20 kHz frequency, combined with a swirler and an anchoring component that ensures geometric stabilization of the arc column. This configuration enabled stable plasma discharge under high-temperature (>200°C) and high-pressure (>2 bar) conditions. The propulsion performance of the plasma reactor was significantly improved by rapidly heating the discharge gases, which were then accelerated to supersonic speeds through a De-Laval nozzle. In the electrochemical operation mode, this process led to consistent enhancements in both chamber pressure and characteristic velocity, achieving approximately 1.4- and 2-fold increases, respectively, compared to the chemical mode (without plasma discharge). The novel propulsion concept can provide a universally applicable solution capable of enhancing the performance of chemical propulsion systems with plasma discharge.

Nomenclature

 A_t = nozzle throat area, m²

 C^* = characteristic velocity, m/s

 $I_{\rm arc}$ = arc current, A

 $I_{\rm Rms}$ = root-mean-square value of arc current, A

 \dot{m} = mass flow rate, kg/s

P = average value of applied power, W P_c = plasma reactor chamber pressure, bar

T = time interval for the measurement of electrical data, s

 $T_{c,\text{exp}}$ = measured chamber temperature, °C $T_{c,\text{theo}}$ = theoretical chamber temperature, °C

 T_{room} = room temperature, °C

t = time, s

 t_0 = initial measurement time, s

 $V_{\rm arc}$ = arc voltage, V

 $V_{\rm Rms}$ = root-mean-square value of arc voltage, V

 η_{temp} = temperature efficiency, %

I. Introduction

THE rapid growth of the launch vehicle market in recent years has decreased the cost to orbit, significantly increased the versatility of space missions, and expanded the range of mission

Received 8 April 2024; accepted for publication 13 April 2025; published online 13 May 2025. Copyright © 2025 by the American Institute of Aeronautics and Astronautics, Inc. All rights reserved. All requests for copying and permission to reprint should be submitted to CCC at www. copyright.com; employ the eISSN 1533-385X to initiate your request. See also AIAA Rights and Permissions https://aiaa.org/publications/publish-with-aiaa/rights-and-permissions/.

*Doctoral Student, Department of Mechanical Engineering, 77 Cheongam-Ro, Nam-Gu; jackzigzag@postech.ac.kr. Student Member AIAA.

[†]Doctoral Student, Department of Mechanical Engineering, 77 Cheongam-Ro, Nam-Gu; tjdgus@postech.ac.kr. Student Member AIAA.

[‡]Assistant Professor, Department of Mechanical Engineering, 77 Cheongam-Ro, Nam-Gu; annalee@postech.ac.kr (Co-Corresponding Author).

§Postdoctoral Researcher, Department of Plasma Engineering, 156 Gajeongbuk-Ro, Yuseong-Gu; jwkim95@kimm.re.kr. Member AIAA.

[†]Senior Researcher, Department of Plasma Engineering, 156 Gajeongbuk-Ro, Yuseong-Gu; hjkang@kimm.re.kr Member AIAA (Corresponding Author).

orbits. Major cases include small satellite constellations in the low Earth orbit, interplanetary orbital missions, and deep space exploration [1–3]. For such missions, small-scale thrusters that provide multithrust levels with sufficient efficiency are critical for the success of the missions. To date, small monopropellant thrusters utilizing hydrazine have been widely commercialized. Despite its widespread use, the high toxicity of hydrazine requires significant costs due to specialized purification infrastructures for handling [4]. To address these issues, recent studies were focused on high-performance green monopropellants that can replace hydrazine, thereby improving both the cost efficiency and environmental sustainability.

Green monopropellants are typically classified into ionic monopropellants and green oxidizers, both of which operate through catalytic decomposition or combustion processes. Representative ionic monopropellants include hydroxylammonium nitrate (HAN) and ammonium dinitramide (ADN), while nitrous oxide (N2O) and hydrogen peroxide (H₂O₂) are common examples of green oxidizers. The properties of these monopropellants are summarized in Table 1 [5]. Ionic monopropellants have garnered attention due to their high adiabatic flame temperatures, which enable a high specific impulse. Furthermore, their high density reduces the total propulsion system mass, making them ideal for compact designs. However, they require the catalyst bed to be preheated, often above 250°C, necessitating additional heating systems [6,7]. Nitrous oxide offers the advantage of being self-pressurizing but presents drawbacks such as requiring catalyst bed preheating to initiate decomposition and having relatively low density [8]. In contrast, hydrogen peroxide decomposes rapidly upon contact with a catalyst, enabling cold starts without preheating, and has a high density, which facilitates the construction of compact propulsion systems [9]. However, it exhibits relatively low specific impulse, which has motivated the exploration of various technical approaches to overcome this

Efforts to enhance the performance of existing green monopropellants have largely focused on adjusting the design and materials of catalyst beds to increase decomposition rates and catalyst durability of monopropellant thrusters [12–14]. For hydrogen peroxide, blending with hydrocarbon fuels such as ethanol or tetraglyme has been shown to improve specific impulse by increasing the temperature of the catalytically decomposed gases [15,16]. Similarly,

Table 1 Comparison of green monopropellants

	Isp,	Density, kg/m ³	Catalyst preheating temperature, °C	Adiabatic flame temperature, °C
H ₂ O ₂ (100%) ^a	185	1.44		1004
N ₂ O [5,8,10]	206	0.79	250	1640
ADN (LMP-103s) [5,6,10]	254	1.31	350	1725
HAN (AF-M315E) [5,7,10]	257	1.47	285	1893

^aThe vacuum-specific impulse was calculated for a chamber pressure of 10 bar and a nozzle expansion ratio of 50 using Chemical Equilibrium with Analysis [11].

blending ADN with hydrogen peroxide or tetraglyme has been experimentally demonstrated to enhance specific impulse and reduce the catalytic decomposition response time, while requiring lower preheating temperatures [17,18]. Despite these advancements, the above chemical methods face challenges in maintaining long-term catalyst performance and stability due to prolonged exposure to high decomposition and combustion temperatures. Furthermore, such approaches are inherently constrained by the heat release from monopropellants chemical reactions, which imposes an upper limit on achievable gas temperatures and specific impulse.

For electrothermal methods including resistojets, arc jets, and microwave electrothermal thrusters, it is possible to supply additional electric power to heat propellants [19]. Recent research focusing on the enhancement of ignition and propulsion performance by applying plasma discharge onto ionic monopropellants has drawn significant attention. Various kinds of plasma sources, such as arc, (nano-)pulse discharge, and microwave have recently been studied as ignition methods for ADN [20-22] and HAN [23-25]. The direct transfer of thermal energy of plasma to the ionic monopropellants can enable fast and reliable ignition without a preheating process for the catalyst bed. In some cases, arc plasma was continuously discharged to improve both ignition and thrust performance of the thruster [26]. The previous studies indicate that utilizing additional electrical energy can be one of the options to achieve higher specific impulse by further increasing the temperature of the working gases beyond the limitation of their chemical energy.

The present research proposes a novel concept of electrochemical propulsion system using hydrogen peroxide as a green monopropellant. Rotating gliding arc (RGA) plasma was introduced to address the inherently low specific impulse of hydrogen peroxide, which differs from the plasma sources in the conventional electric propulsion systems. Compared with microwave plasma, arc-based plasma does not require the sophisticated circuitry and impedance matching necessary for high-frequency discharges, and direct discharge to the medium through electrodes allows for a simpler and more reliable system configuration. Moreover, the rotating motion of arc can contribute both to maintain uniform heat distribution in space and to minimize the electrode wear rate. When RGA is applied to an electrothermal propulsion system, it is anticipated that these characteristics could allow the system to operate uniformly with high efficiency over extended periods. In this study, the performance improvement of the novel propulsion system using RGA plasma was experimentally confirmed through repeatable hot-firing tests. In the previous research [27], the applicability of RGA to propulsion systems was proven where the CO₂-based RGA was stably discharged at the high pressure (>2 bar) to form a supersonic flow. The change in the chamber pressure before and after the plasma discharge was also measured to assess the potential for performance improvement. Furthermore, the electrical characteristics of the RGA were analyzed by measuring voltage and current waveforms at the reactor. To the best of our knowledge, this is the first attempt to utilize the catalytically decomposed gases of hydrogen peroxide as plasma-forming gases. From this perspective, the proposed electrochemical propulsion method is highly innovative, as it employs plasma discharge to enhance the performance of hydrogen peroxide thrusters.

II. Materials and Methods

A. Catalyst Fabrication

In this study, 88 wt% of hydrogen peroxide was selected as a green propellant to demonstrate the novel concept of an electrochemical hybrid propulsion system composed by both a catalytic and plasma reactor, as it can be implemented through a simple system. The density of the propellant is 1.383 g/cm³. The adiabatic decomposition temperature was theoretically estimated by NASA Chemical Equilibrium with Applications with a chamber pressure of 3 bar, resulting in approximately 707.5°C [11]. The fabrication of the pellet-type catalyst, which was subsequently loaded into the catalyst reactor, is detailed in this section. The monopropellant thruster's catalyst bed must maintain a high specific surface area when withstanding high propellant flow rates, temperatures, and pressures. Typically, the bed consists of an active material and a catalyst support. For this study, γ -Al₂O₃ was selected as the catalyst support due to its excellent mechanical properties and ability to retain a high specific surface area under the decomposition temperature of hydrogen peroxide [28,29]. Additionally, γ -Al₂O₃ exhibits strong adhesion to metals and its durability and thermal resistance can be enhanced through doping with elements such as Ba [30] or La [31], making it suitable for various green monopropellants. Commonly used active materials for hydrogen peroxide decomposition include Ag [32], Ir [29], Pt [33], and MnO_x [34,35]. In this study, MnO_x , a cost-effective material with relatively lower reactivity, was doped onto the catalyst support as part of the conceptual demonstration. Future studies should explore the use of precious metal-based active materials with higher reactivity to further optimize the catalyst bed's performance.

The fabrication method adopted for catalyst preparation was based on the previous research [34,35]. Initially, $1/8 \text{ in } \gamma\text{-Al}_2\text{O}_3$ pellets (Alfa-Aesar, USA) were ground, and particles with diameters of 1.00-1.18 mm were selected. In previous studies on thrusters using pellet-type catalysts, active materials have typically been loaded onto the support in concentrations of 20-30 wt% [28,30,34,35]. Accordingly, MnO_x was doped onto the alumina support at a target concentration of 30 wt%. To this end, 20 g of γ-Al₂O₃ granules were mixed with 70.5 g of a 40 wt% NaMnO₄ aqueous solution (Dongmoon Chemical Co., Republic of Korea) until the granules were fully wetted. Subsequently, the mixture was heated at 120°C for 22 h in a convection oven to ensure manganese impregnation. The dried catalyst was then placed in an alumina crucible and calcined at 500°C for 5 h in an electric furnace. The final step involved washing and redrying the catalyst at 120°C for 22 h. The doping concentration and specific surface area of the fabricated pellet-type catalyst were measured. In the MnO_x/Al_2O_3 catalyst, the doping concentration of manganese was measured by inductively coupled plasma optical emission spectrometry (ICP-OES) with an iCAP6300 instrument (Thermo Fisher Scientific Co., USA). ICP-OES requires a sample in a liquid state. We added 50 mg of MnO_x/Al_2O_3 pellet to a mixture of 0.5 mL of sulfuric acid and 5.0 mL of aqua regia and then heated at 170°C for 30 min to dissolve the pellet. Subsequently, the concentration of doped manganese was measured by dilution by a known volume of water. This process was repeated three times to ensure accuracy, and the average concentration of manganese was found to be 26.0%, similar to the target value. In addition, the specific surface area of the MnO_x/Al₂O₃ catalyst was determined by utilizing the Brunauer-Emmett-Teller method using a Tristar II 3020 instrument (Micromeritics, USA). During the measurement procedure, the nitrogen adsorption was conducted at an environment of 73 K. This process was also repeated three times, and the average specific surface area was measured to be 70.63 m²/g. Figure 1a presents the MnO_x/Al_2O_3 catalyst granules in the catalyst reactor. The reactor chamber had a diameter and length of 20 and 30 mm, respectively, thus loading 20.1 g of catalyst granules. Figure 1b presents an overview of the catalyst reactor.

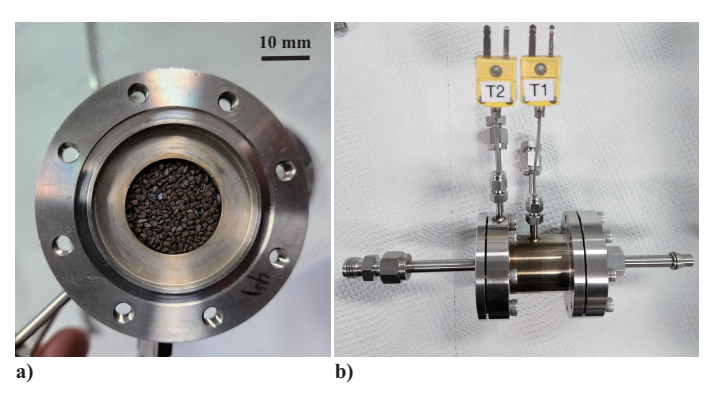


Fig. 1 a) Fabricated MnO_x/Al₂O₃ catalyst granules with the catalyst support size of 1.00–1.18 mm and b) small-scale catalyst reactor.

B. Design Concept of Plasma Reactor

Figure 2 provides the technical information for the design concept of the plasma reactor. The plasma reactor was empirically designed to form a supersonic flow by uniformly heating the decomposed hydrogen peroxide gas injected from the catalyst reactor to the inlet of the plasma reactor. The catalyst reactor was integrated with the plasma reactor for the purpose of firstly decomposing hydrogen peroxide to produce the plasma forming gas. The other components of the plasma reactor were a discharge chamber, an anchoring part, and a secondary chamber.

Discharge chamber: For the initiation of arc discharge in the plasma reactor, the high-voltage line of the power supply was connected to the water-cooled copper electrode to supply an alternating current flow. In addition, the stainless steel discharge chamber body serves as the ground, and a ceramic part was used to electrically isolate the aforementioned two components. The copper electrode, designed in a stick shape, was water-cooled to mitigate erosion caused by the arc spot. For the grounded electrode, water cooling was unnecessary due to the thickness of the reactor body. The discharge gap between the head of the cone-shaped copper electrode and the discharge chamber body for the RGA ignition was designed as 0.7 mm. The open-circuit voltage of the power supply was set as 6 kV, and the discharge frequency was fixed as 20 kHz. A customized alternating current power supply was developed by PowerFactors Co., Ltd. in the Republic of Korea. The rated plasma power was controlled by adjusting the set current, whereas the operating voltage was passively determined based on the load characteristics. To even out spatial heat distribution and reduce electrode wear, the arc was rotated by injecting decomposed hydrogen peroxide gas through a swirler. This also can stabilize the arc by inducing the gliding motion of the arc in the length direction of the electrode and enables efficient heating of the working gas. The swirler was constructed by drilling three holes, each with a diameter of 2 mm, in a direction perpendicular to the electrode and placing it at a distance of 6 mm from the center.

Anchoring part: In general, under high pressure conditions, it is difficult to maintain a stable plasma discharge due to the increased frequency of molecular collisions. A structural design that can extend the length of the arc and geometrically stabilize the RGA plasma under high-pressure conditions is required. To achieve this, a stepped structure was placed between the anchoring part outlet and the secondary chamber inlet, as shown in Fig. 2. The arc spot on one side of the arc column was located toward the tip of the high-voltage electrode, and the remaining arc spot rotates continuously along the edge of the anchoring part (ground). This allows the arc column to be anchored to the part before the chamber pressure rises. Downstream of the 17 mm inner diameter discharge chamber, a structure with an anchoring part throat diameter narrowed to 4.5 mm and then expanded to 6.5 mm was placed. For the convenience of machining processing (smoothly curved), the convergence and divergence angles were set to 45 and 24 deg, respectively.

Secondary chamber: When the arc column was stably located at the anchoring part, the diffusive plasma jet could form in the secondary chamber due to the mass diffusion of the energetic species from the arc column to the surrounding ambient. As a result, the ionized and excited gas species filled with the volume of the secondary chamber. Accordingly, the bulk gas temperature and pressure inside of the secondary chamber were simultaneously increased. The De-Laval nozzle was located downstream of the secondary chamber and served to accelerate the flow of high-temperature and pressure gas to supersonic speed. The nozzle throat diameter was designed as 2.2 mm, with the throat length being approximately twice its diameter, and the exit diameter was designed as 2.5 mm. The convergence and divergence angle were set to 60 and 15 deg, respectively.

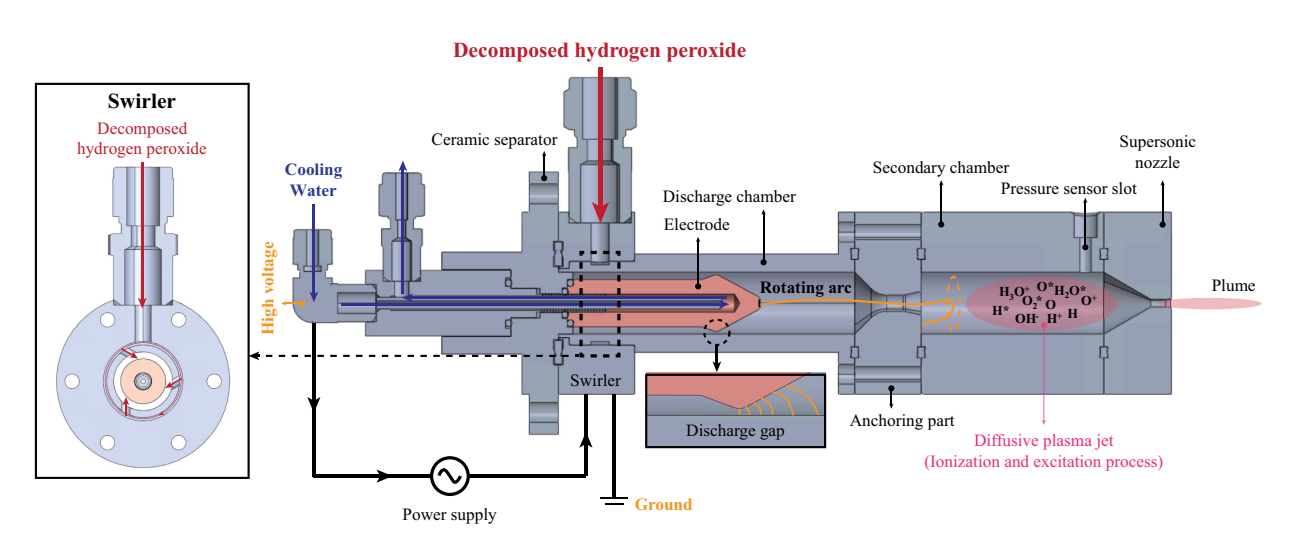
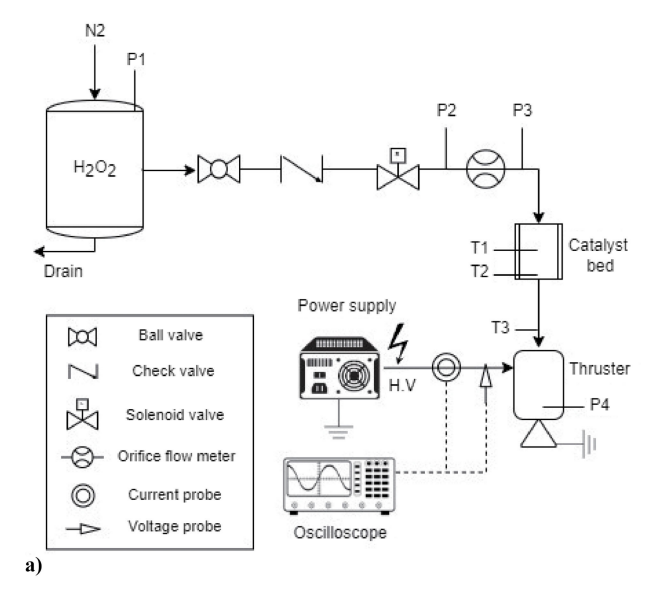


Fig. 2 Schematic drawing of plasma reactor.

C. Hot-Firing Test Apparatus

Figure 3 presents the hot-firing test apparatus. The propellant tank was pressurized with N2 gas. An orifice flow meter with a diameter of 0.6 mm was connected downstream of the tank to estimate the mass flow rate of the propellant depending on the magnitude of the differential pressure (P2 and P3) with the pressure level (P1) of the tank. For the catalyst bed in the reactor, two K-type thermocouples were placed at the middle (T1) and outlet (T2) of the reactor. The decomposed hot gases, steam, and oxygen, were supplied directly to the swirl injector of the plasma reactor. The inlet temperatures of the gases were measured by using K-type thermocouples (T3). In this study, there was no insulation part downstream from the catalyst reactor. One pressure sensor (P4) was placed at the discharge changer to investigate the pressure variations either with ("electrochemical operation mode") or without ("chemical operation mode") the plasma discharge. Herein, the direct measurement of the temperature inside the chamber was not attempted, considering the probability of striking a high-voltage arc at the tip of the thermocouple protruding inside the chamber. The model of the pressure sensors was PSCD0010BCPG (Sensor System Technology Co., Ltd). A high-voltage probe (Tektronix P6015A) and current probe (Tektronix TCP0150) were used to measure the electrical data of the RGA. Electrical data were monitored using an oscilloscope (Tektronix MSO44 4-BW-200). Temperature and pressure data were recorded using a GRAPHTEC GL-840 data logger at a sampling rate of 10 Hz. The operation sequence of the electrochemical propulsion system is as follows: The catalyst bed for hydrogen peroxide decomposition was located upstream of the plasma reactor. The gas mixtures, H₂O and O₂, produced by hydrogen peroxide decomposition were directly supplied to the plasma reactor as plasma-forming gases. When the pressure level (P4) of



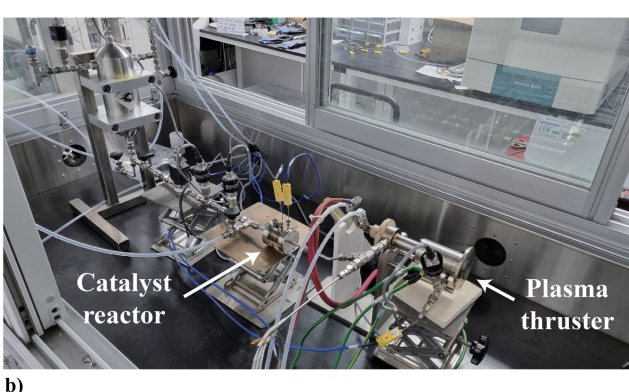


Fig. 3 $\,$ a) Schematic view and b) actual image of electrochemical hybrid propulsion system.

the plasma reactor was achieved at steady state, arc discharge was initiated using the high-voltage power supply. The RGA plasma discharge was triggered at the gap in the beginning. Subsequently, the arc column was immediately elongated along with the swirling motion of the gases and stably rotated around the anchored part. At the end, the superheated discharge gases were ejected from the discharge chamber.

III. Results and Discussion

A. Chemical Operation Mode

Figure 4 presents the experimental results of the catalyst reactor operation ("Test set 1") conducted at a relatively low level of the tank pressure. The timescale (x-axis) shown indicates the cumulative time from the instant at which the propellant supply valve was opened (0 s), thus leading to the immediate injection of the propellant into the catalyst reactor. The inlet pressure (pressure level of the propellant tank, P1) was set to 3.5 bar, and the propellant was continuously injected into the catalyst reactor for 20 s. Figure 4a shows the temperature data measured at various locations within the system. The maximum temperature (T1), measured in the middle of the catalyst reactor, reached 535.5°C. Using Eq. (1) and the adiabatic decomposition temperature of 88 wt% hydrogen peroxide, the temperature efficiency was calculated to be 74.80%.

$$\eta_{\text{Temp}} = (T_{c,\text{exp}} - T_{\text{room}}) / (T_{c,\text{theo}} - T_{\text{room}})$$
 (1)

The outlet temperature (T2) was lower than that of the middle of the reactor. Right after that, an enormous amount of heat loss to the ambient air might cause the further temperature decrease at the outlet of the catalyst reactor. This heat dissipation is attributed to the high surface-to-volume ratio inherent to small-scale systems. In this light, it was also reasonable that the maximum decomposition temperature measurable in the catalyst reactor would be lower than the value of the theoretical estimation due to heat loss. Constructing the catalyst bed using materials with lower thermal conductivity could mitigate this heat loss. From a conservation point of view, the size of the catalyst bed was intentionally designed to be larger

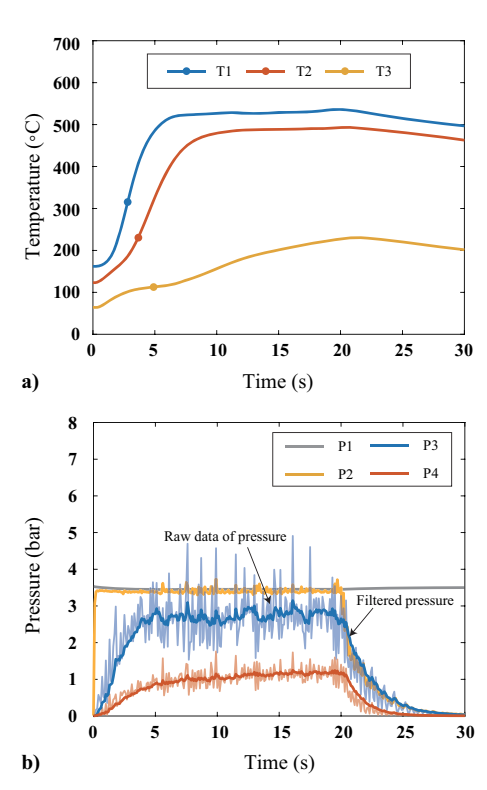


Fig. 4 Measurement data of a) temperature and b) pressure during Test Set 1 operated in the chemical operation mode.

 (1.0 (g/s)/cm^3) than a target value $(2.62 \text{ (g/s)/cm}^3)$ in terms of catalyst capacity [36]. Under low flow rate conditions and due to the relatively large size of the reactor, the gas, likely exhibiting a higher decomposition temperature in the upper section of the catalyst bed, could be expected to cool as it flows to the middle section, where the T1 sensor is located. Based on these assumption, the hydrogen peroxide decomposition rate in the catalyst bed was conservatively estimated to be at least the same as the temperature efficiency, i.e., 74.80%. However, precise verification of this assumption was limited by the current experimental setup. Future studies should focus on optimizing the material and design of the reactor and catalyst bed to minimize heat dissipation, as well as on adjusting the experimental setup to directly measure the decomposition rate. This could involve sampling gas downstream of the catalyst bed and measuring the oxygen generation rate. The inlet temperature (T3) of the plasma reactor exceeded 100°C in 2.7 s, indicating that the gas mixture (H₂O and O₂) produced by hydrogen peroxide decomposition could be injected into the plasma reactor in gaseous state without any condensation problems, thereby preventing the discharge instability caused by liquid-gas two-phase flow. To ensure that gas temperatures approach the adiabatic decomposition temperature, gas travel distances must be minimize by further optimizing the catalyst bed and integrating it with the plasma reactor.

Figure 4b provides the pressure data measured at each location. The pressure data measured at the catalyst bed and the plasma reactor were plotted, including both raw data and trend lines smoothed using a low-pass filter. Pressure perturbations observed at *P*3 in the catalyst reactor were attributed to the violent decomposition of hydrogen peroxide in the catalyst reactor. Typically, to suppress low-frequency

pressure perturbations, the feed system should be isolated from the catalyst bed, which requires an injector capable of inducing a pressure drop of 5–20% of the catalyst bed pressure [37]. Incorporating an orifice injector with an appropriately sized diameter at the upper section of the catalyst bed can address this instability by ensuring sufficient pressure drop. The steady-state chamber pressure (*P*4) of the plasma reactor was reached at approximately 1.09 bar. The average mass flow rate was measured as 2.67 g/s, and the raw data for the entire duration are shown in Fig. A1a in Appendix A.

B. Electrochemical Operation Mode

Based on the experimental data of the low-pressure demonstration of the chemical operation mode, the feasibility of the electrochemical operation mode was accessed in three different experimental sets. Considering the pressure drop in the catalyst reactor, it was essential to increase the input pressure (*P*1) not only to maintain sufficient chamber pressure (*P*4) for the generation of supersonic flow at the nozzle, but also to minimize pressure perturbations at the inlet of the plasma reactor. Therefore, "Test Set 2" was conducted with the tank pressure of 5.0 bar, and "Test Set 3" was subsequently performed with the tank pressure of 6.0 bar. The operating duration was set for 30 s in the both cases. The flow rate data during the operation of "Test Sets 2–3" are shown in Figs. A1b and A1c in Appendix A.

Figure 5a provides the representative images obtained from the electrochemical operation mode test. In the chemical operation mode, only hydrogen peroxide decomposition gases were ejected from the plasma reactor (Fig. 5a1). Upon applying the electric power to initiate plasma discharge, the system entered the electrochemical operation mode. The indication of the beginning on the

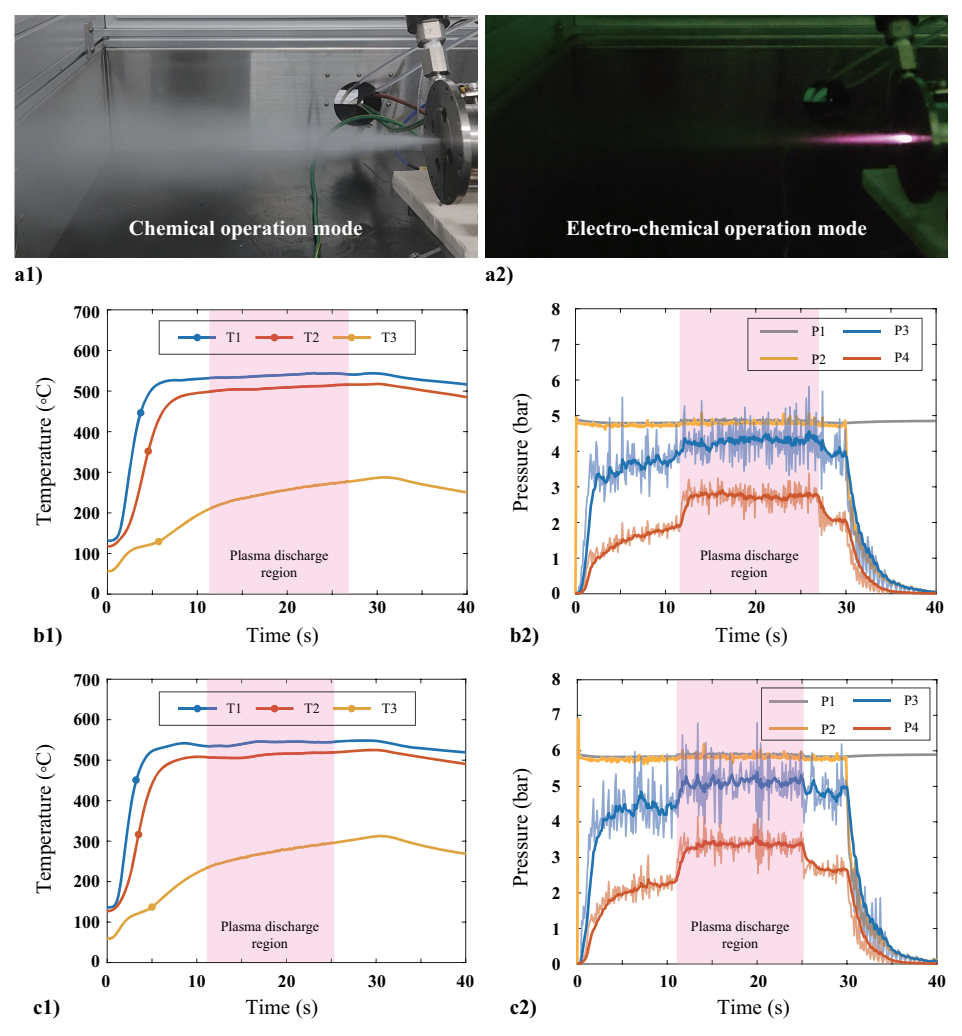


Fig. 5 Images captured during a1) chemical and a2) electrochemical operation, b1, c1) temperature, and b2, c2) pressure measured during "Test Set 2" and "Test Set 3."

electrochemical operation mode was the generation of the violetcolored plasma jet at the nozzle (see in Fig. 5a2). Interestingly, when the plasma discharge was maintained, the visible emission of the plasma plume appeared purple. Due to the limitations of the experimental setup in terms of optical spectroscopy, it was difficult to quantitatively characterize the optical emissions of the plasma plume. Nevertheless, it was reasonable that the emissions could be related to ionized species in the plasma, especially hydrogen and oxygen. Both species were the major chemical components of the decomposed gases, and some parts of their emission spectra were included in the ultraviolet region (see Appendix B).

Figures 5b and 5c denotes the measurement data of temperature and pressure in "Test Sets 2 and 3," respectively. The temperature profiles shown in Figs. 5b1 and 5c1 of the catalyst reactor were very similar to those of "Test Set 1," suggesting the complete decomposition of the propellants. The inlet temperatures of the plasma reactor became higher, reaching up to 287.9 and 312.7°C, respectively, as the mass flow rates of the propellant were increased with the higher input pressures. As shown in Figs. 5b and 5c, the plasma discharges were initiated at 11.6 s in "Test Set 2" and 11.0 s in "Test Set 3." The time duration of plasma discharge was marked as "Plasma discharge region" in the figures. Figures 5b2 and 5c2 presents the pressure measurement results of the test sets. During the plasma discharge in "Test Set 2," the chamber pressure (P4) of the plasma reactor rapidly increased from 1.90 to 2.75 bar, which represents an increment of 44.8%. In the case of "Test Set 3," the chamber pressure increased from 2.34 to 3.36 bar, which represents an increment of 43.6%. It can be inferred that the pressure rise was associated to an increase in the temperature of the gases inside the reactor with the plasma discharge. With the design of the supersonic nozzle, it can be theoretically assumed that the choked flow is formed at the nozzle throat when the chamber pressure reaches a higher pressure by a factor of approximately 1.81 bar compared to the exit pressure of the nozzle. Considering that the pressure of the nozzle exit was atmospheric pressure (1 atm), it can be said that the pressure differences for the choked flow condition at the nozzle was fulfilled in all the tests of the electrochemical operation mode. Although the Mach discs were not directly observed in the plasma plume with the naked eyes due to its high emission intensity, the pressure level of the chamber could guarantee the formation of plasma supersonic flow at the nozzle exit. The successful achievement of the electrochemical operation mode verified that the alternating-current RGA could be sustained even for the high temperature (>200°C) and pressure (>2 bar) environments based on the gaseous mixture of H₂O and O₂. The rapid pressure rise of the chamber (P4) during the electrochemical operation mode influenced the pressure differences on the inlet of the catalyst reactor (see P3 in Figs. 5b2 and 5c2, leading to the slight reduction of the total flow rate. The propellant mass flow rate decreased from 3.32 to 2.33 g/s in "Test Set 2" and from 3.78 g/s in "Test Set 3" during the plasma discharge. Although the thrust could not be directly measured due to the experimental limitations, such pressure jumps are directly linked to an increase in thrust. Given that the chamber pressure of the plasma reactor was increased, despite the decrease in the flow rate, the fact suggests that the electrochemical operation mode required less amount of the propellant than that of the chemical operation mode to generate an equivalent amount of thrust.

$$C^* = P_c A_t / \dot{m} \tag{2}$$

To evaluate the propulsion characteristics of each mode, the characteristic velocity (C^*) was experimentally calculated using Eq. (2) based on the dimensions of the nozzle geometry described in Sec. II.B. The characteristic velocity increased from 217.40 to 447.59 m/s during the plasma discharge in "Test Set 2," and likewise, increased from 235.54 to 456.57 m/s in "Test Set 3." The results represent that the increment of the propulsive performance was approximately more than two-fold in the electrochemical operation mode. The theoretical characteristic velocity of the reactor using 88 wt% of hydrogen peroxide under the chemical operation mode, where the chamber pressure of 3 bar and the nozzle exit

pressure of 1 atm, was approximately 918.77 m/s [23]. However, the theoretical value deviated from the experimental results. In the present study, the physical separation between the catalyst and plasma reactor seemed to be the primary cause of the discrepancy as it led to considerable heat loss from the decomposed gases. Consequently, the inlet temperature of the plasma reactor was significantly low. A future study integrating these two components could address these challenges. From the same fundamental principle, it is expected that the characteristic velocity can be boosted with the application of RGA.

The experiment of "Test Set 4" was performed to confirm the reproducibility of the novel concept under the highest operable input pressure condition (P1) of 6.0 bar, which was identified with the test condition of "Test Set 3." Figure 6 presents the experimental results of "Test Set 4." The flow rate data for "Test Set 4" was also provided to Fig. A1d in Appendix A. The test video for "Test Set 4" was provided in the Supplementary Material. In this case, the total operating duration was extended for 40 s and the plasma discharge was maintained from 11.5 to 34.8 s. The temperature profiles in the catalyst reactor and plasma reactor shown in Fig. 6a were very similar to those obtained in "Test Set 3." The chamber pressure was also increased from 2.30 to 3.32 bar, and the increment of the pressure was approximately 44.56%. It was found that the result closely corresponded to the data in "Test Set 3." The variation of the

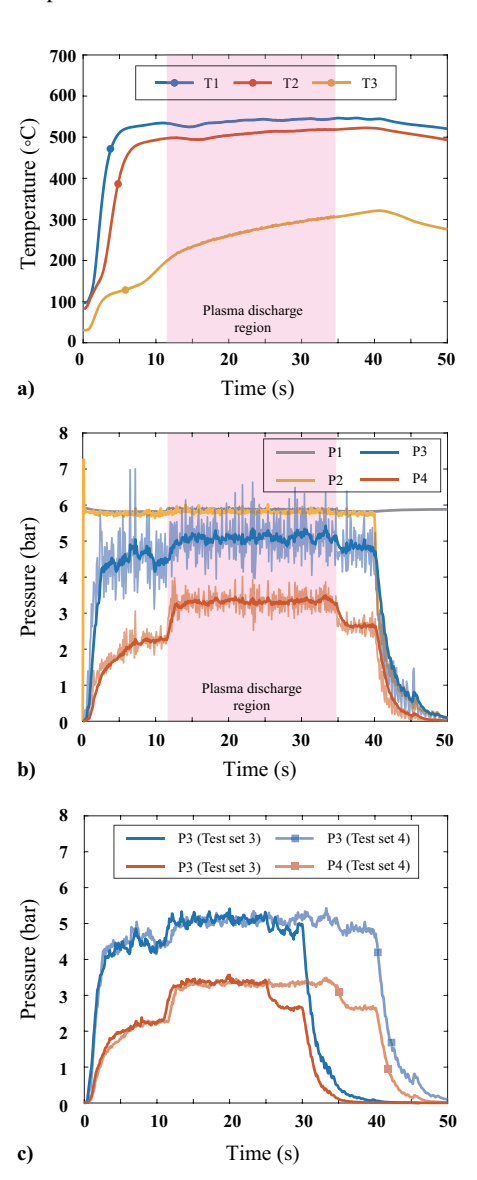


Fig. 6 a) Temperature and b) pressure measured during "Test Set 4," c) comparison of the plasma reactor's pressure profiles obtained during "Test Set 3" and "4."

mass flow rate of the propellant before and after the plasma discharge was estimated from 3.56 to 2.79 g/s. In Fig. 6c, the filtered pressure data obtained in "Test Set 4" were intentionally superimposed with the data of "Test Set 3" for easy comparison. The reliability of the experimental data was clearly confirmed because the pressure profiles measured were almost identical throughout the entire operation time. Additionally, the characteristic velocity calculated in "Test Set 4" increased from 244.89 m/s (chemical operation mode) to 454.16 m/s (electrochemical operation mode). The result was also very similar to that of "Test Set 3." In summary, the reliable verification on the novel concept of the electrochemical propulsion is implied that the application of rotating gliding arc for stable thrust control is technically feasible.

Figure 7 provides the electrical characteristics of the plasma discharge obtained from "Test Set 4." The current and voltage waveforms appeared in a sinusoidal form (Fig. 7a), and their frequency was determined from the alternating discharge frequency of the power supply. When the zero-crossing of the voltage waveform occurred, a sharp increase in voltage was observed at the discharge gap, thus resulting in the inception of the arc discharge. The breakdown voltage of the plasma reactor was approximately 2 kV in the electrochemical operation mode in each cycle. When the discharge was initiated, the insulation between the electrodes broke down, thus allowing for current to flow. This current flow caused a rapid voltage drop. Immediately after the breakdown of the spatial insulation around the discharge gap, a momentary spike in the current was followed; however, the current assumed a stable sinusoidal shape shortly thereafter. As the current was stabilized, the voltage was stably converged to a certain value. The appearance of the voltage peak following each zero-crossing phase indicates that the arc column completely dissipated just before the onset of the subsequent arc redischarge cycle. Given the well-known memory effect associated with arc discharge phenomena, charged particles remaining from the previous discharge can facilitate smooth redischarge at a relatively low voltage if they exist near the discharge site. In order words, the life time of the ionized and excited species produced by the previous arc discharge event could influence on the onset voltage of the subsequent redischarge event. One challenge for achieving

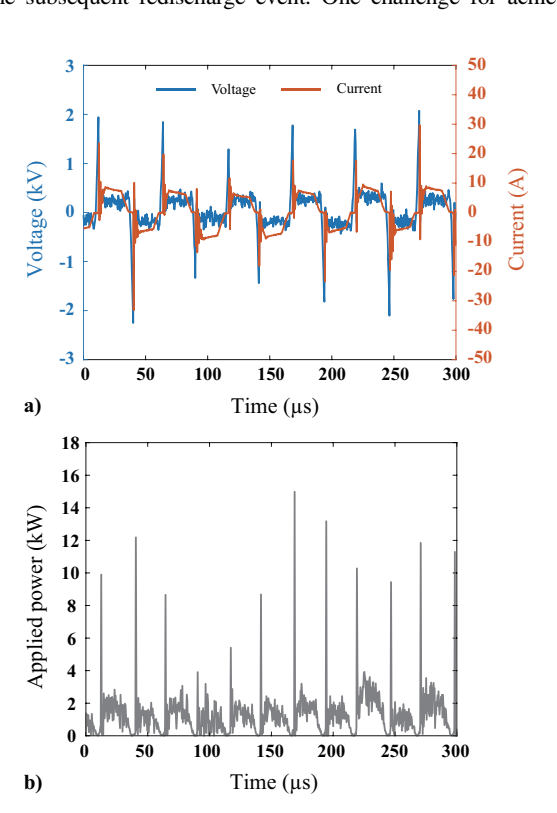


Fig. 7 Variations of electric wave forms: a) voltage and current and b) applied power, driven by alternating current power supply with designed frequency of $20~\mathrm{kHz}$.

such smooth redischarge of the arc in every cycle is related to a high pressure environment. In this work, the chamber pressure during the electrochemical operation mode was higher than the atmospheric pressure (1 atm). In fact, these high pressure conditions in the discharge chamber make the initiation of arc discharge more difficult. Nevertheless, the high-voltage AC waveform was capable of continuously generating discharges, even in the electrochemical operation mode where the chamber pressure was higher than the atmospheric pressure by a factor of approximately three times. The behaviors of the current-voltage waveform were critical for determining the power waveform as shown in Fig. 7b. The peak value of the power wave does not represent the actual effective power applied to the plasma reactor. The observed voltage and current were calculated using Eqs. (3) and (4) as $408V_{\rm rms}$ and $6.37A_{\rm rms}$, respectively. This calculation allows for the determination of the average power, which, according to Eq. (5), was approximately 1.25 kW. Design improvements should be focused on minimizing the sharp peaks of electric waves observed after the zero-crossing phase.

$$V_{\text{RMS}} = \sqrt{\frac{1}{T} \int_0^T V_{\text{arc}}^2(t) \, \mathrm{d}t}$$
 (3)

$$I_{\text{RMS}} = \sqrt{\frac{1}{T} \int_0^T I_{\text{arc}}^2(t) \, \mathrm{d}t}$$
 (4)

$$P = \frac{1}{T} \int_{t_0}^{t_0+T} V_{\text{arc}}(t) \times I_{\text{arc}}(t) \, dt \tag{5}$$

IV. Conclusions

In the present research, the novel concept of hydrogen peroxide based electrochemical propulsion with rotating gliding arc (RGA) was experimentally demonstrated. The 88 wt% of hydrogen peroxide was catalytically decomposed to supply the plasma forming gases in the plasma reactor. Depending on the application of plasma discharge, the operation mode of the plasma reactor was distinguished: without plasma discharge (chemical operation mode) and with plasma discharge (electrochemical operation mode). The propulsive performance of the chemical operation mode and the electrochemical operation mode were quantitatively evaluated. The plasma discharge contributed to increase the chamber pressure approximately 1.4 times compared to that of the chemical operation mode. It is speculated that the arc plasma primarily served as a heat source, especially under high-pressure discharge conditions. Meanwhile, the possibility on the occurrence of any plasma chemistry was excluded because only one reactant (hydrogen peroxide) was introduced and plasma chemistry under such high-pressure conditions was beyond the scope of this research. The experimental results of "Test Sets 2-4" represent that the increment of the propulsive performance was approximately more than two-fold in the electrochemical operation mode in terms of characteristic velocity. It was also confirmed that the high-voltage AC waveform was capable of continuously generating discharges, even in the electrochemical operation mode where the chamber pressure was higher than the atmospheric pressure by a factor of approximately three times. The fact proves that the proposed RGA-based plasma reactor can sustain a stable discharge condition for sufficient duration with the gas mixtures produced by the catalytic decomposition of hydrogen peroxide exceeding 200°C and 2 bar. Additionally, the superheated plasma gases in the chamber were successfully accelerated to supersonic speed through the De-Laval shaped nozzle. Furthermore, the concept of the multimode operations allows for a capability of variable thrust-level controls based on RGA, which can fulfill a wide range of mission requirements. This approach can be extended beyond the use of hydrogen peroxide. For example, various kinds of cold gases or the decomposed gases generated by energetic ionic monopropellants would be considered as a potential candidate propellant for the application of RGA-based electrochemical

propulsion system. It is believed that the perspective help to boost the versatility of electrochemical propulsion technology based on RGA.

In the current research, there are several limitations on the experimental apparatus. Firstly, the thrust measurement was not possible because of the high-level of system complexity composed of the mechanical (for propellant feeding) parts and electrical (for plasma discharge) parts. Secondly, the temperature of the decomposition gases ejected from the catalyst reactor underwent a rapid decrease due to heat loss as they flowed downstream. As a result, there was a large amount of the discrepancy of the propulsive performance between the experimental results and theoretical estimation in terms of characteristic velocity. In future research, these technical limitations can be resolved by optimizing the integration of both the catalyst reactor and plasma reactor into a single system for simplicity. The design of the electrodes is also important to improve the quality of the arc discharge. Lastly, because direct temperature

measurements inside the chamber are technically challenging, future efforts should focus on accurately diagnosing the high-pressure plasma state generated by the catalytic decomposition of hydrogen peroxide.

Appendix A: Mass Flow Rate of Each Test Set

Figure A1 shows the mass flow rate of hydrogen peroxide fed to the catalyst reactor and plasma reactor during the total operation duration in "Test Sets 1–4." The average mass flow rate of each test set was calculated from the steady state interval.

Appendix B: Optical Emission Observed during the Plasma Mode Operation

Figure B1 indicates the emission spectra of gases. The data was retrieved from the website described in the caption of the figure.

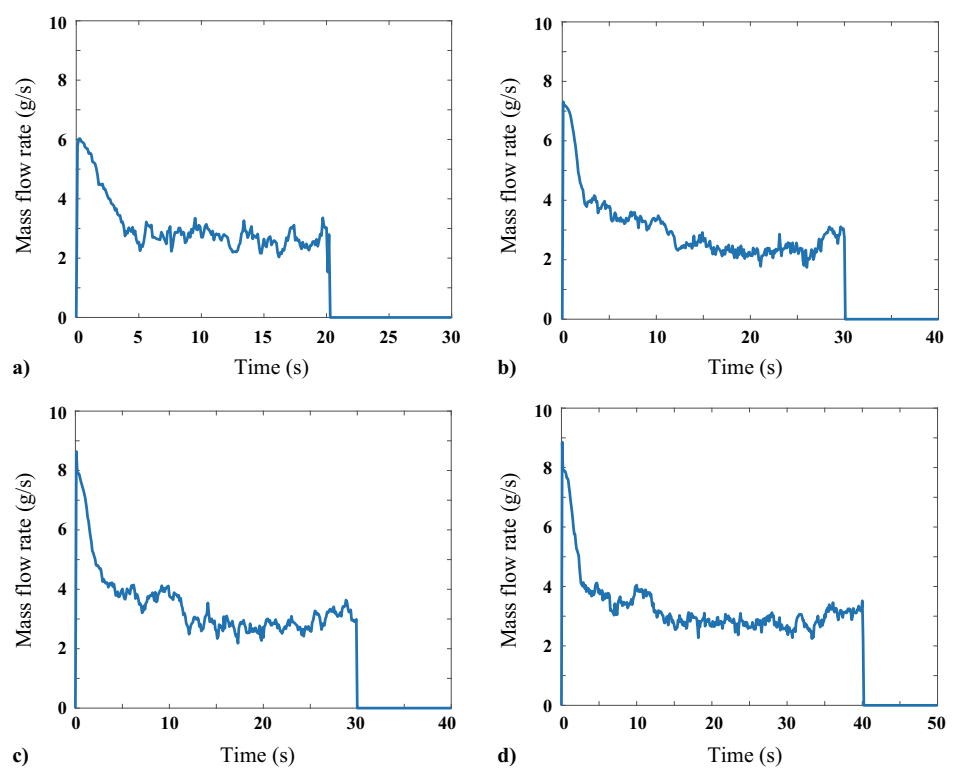


Fig. A1 Mass flow rate of a) Test Set 1, b) Test Set 2, c) Test Set 3, and d) Test Set 4.

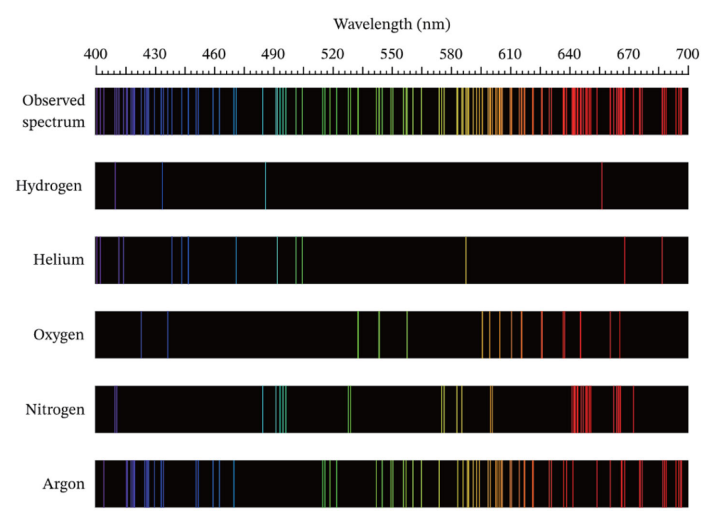


Fig. B1 Emission spectra of gases retrieved from https://www.nagwa.com/en/explainers/469167813067/ (03.04.2024).

According to the emission spectra, oxygen and hydrogen have their own emission spectra around 400–460 nm (ultra-blue violet). The light emission from the supersonic plasma jet was similar to ultra-blue violet color. Considering that the major components of the plasma jet were oxygen and hydrogen, it was inferred that the light emission of the plasma jet might be related to the emission spectra of oxygen and hydrogen in the range of 400–460 nm. In case of hydrogen, three emission wavelengths of the Balmer series (410, 434, and 486 nm) might correspond to the plasma light emission. In case of oxygen, the emission wavelength of (doubly) ionized oxygen, $^1\mathrm{S}_0 \to ^1\mathrm{D}_2$, was 436 nm.

Funding Sources

This work was supported by the National Research Foundation of Korea (NRF) funded by the Korean government (MSIT) (Grant No. RS-2023- 00253824).

Acknowledgment

We would like to thank Editage (www.editage.co.kr) for English language editing.

References

- [1] Malisuwan, S., and Kanchanarat, B., "Small Satellites for Low-Cost Space Access: Launch, Deployment, Integration, and In-Space Logistics," *American Journal of Industrial and Business Management*, Vol. 12, No. 10, Oct. 2022, pp. 1480–1497. https://doi.org/10.4236/ajibm.2022.1210082
- [2] Cervone, A., Topputo, F., Speretta, S., Menicucci, A., Turan, E., Di Lizia, P., Massari, M., Franzese, V., Giordano, C., Merisio, G., et al., "LUMIO: A CubeSat for Observing and Characterizing Micro-Meteoroid Impacts on the Lunar Far Side," *Acta Astronautica*, Vol. 195, June 2022, pp. 309–317. https://doi.org/10.1016/j.actaastro.2022.03.032
- [3] Walker, R., Binns, D., Bramanti, C., Casasco, M., Concari, P., Izzo, D., Feili, D., Fernandez, P., Gil Fernandez, J., Hager, P., et al., "Deep-Space CubeSats: Thinking Inside the Box," *Astronomy & Geophysics*, Vol. 59, No. 5, Oct. 2018, pp. 5.24–5.30. https://doi.org/10.1093/astrogeo/aty232
- [4] Nguyen, H. N., Chenoweth, J. A., Bebarta, V. S., Albertson, T. E., and Nowadl, C. D., "The Toxicity, Pathophysiology, and Treatment of Acute Hydrazine Propellant Exposure: A Systematic Review," *Military Medicine*, Vol. 186, No. 3-4, Feb. 2021, pp. e319–e326. https://doi.org/10.1093/milmed/usaa429
- [5] Sackheim, R. L., and Masse, R. K., "Green Propulsion Advancement: Challenging the Maturity of Monopropellant Hydrazine," *Journal of Propulsion and Power*, Vol. 30, No. 2, 2014, pp. 265–276. https://doi.org/10.2514/1.B35086
- [6] Anflo, K., and Möllerberg, R., "Flight Demonstration of New Thruster and Green Propellant Technology on the PRISMA Satellite," *Acta Astronautica*, Vol. 65, Nos. 9–10, Dec. 2009, pp. 1238–1249. https://doi.org/10.1016/j.actaastro.2009.03.056
- [7] Spores, R. A., "GPIM AF-M315E Propulsion System," 51st AIAA/ SAE/ASEE Joint Propulsion Conference, AIAA Paper 2015-3753, 2015. https://doi.org/10.2514/6.2015-3753
- [8] Li, K., Fang, J., Sun, W., Sun, B., and Cai, G., "Design and Experimental Research of a Sub-Newton N2O Monopropellant Thruster with Inner-Heater," *Chinese Journal of Aeronautics*, Vol. 35, No. 5, 2022, pp. 309–318. https://doi.org/10.1016/j.cja.2021.11.023
- [9] Pasini, A., Pace, G., and Torre, L., "Propulsive Performance of a 1 N 98% Hydrogen Peroxide Thruster," 51st AIAA/SAE/ASEE Joint Propulsion Conference, AIAA Paper 2015-4059, 2015. https://doi.org/10.2514/6.2015-4059
- [10] Remissa, I., Zhenis, T., and Daulet, B., "Propulsion Systems, Propellants, Green Propulsion Subsystems and Their Applications," *Eurasian Chemico-Technological Journal*, Vol. 25, No. 1, 2023, pp. 3–19. https://doi.org/10.18321/ectj1543
- [11] Gordon, S., and McBride, B. J., Computer Program for Calculation of Complex Chemical Equilibrium Compositions and Applications, NASA Reference Publ., Cleveland, OH, 1994, p. 1311.
- [12] Mezyk, L., Kindracki, J., Wacko, K., Wozniak, P., Kostecki, M., Petrus, M., and Bel, F. V., "Initial Investigation of Catalyst Pack for 98%+ Hydrogen Peroxide Satellite Monopropellant Thruster," Acta

- Astronautica, Vol. 225, 2024, pp. 913–927. https://doi.org/10.1016/j.actaastro.2024.09.059
- [13] Kumar, N., Jain, S., Biswas, S., and Kumar, R., "Development of Hydrogen Peroxide Based Micro Thruster Utilizing Biomass-Based Catalyst Bed," *FirePhysChem*, Vol. 2, No. 1, 2024, pp. 45–53. https://doi.org/10.1016/j.fpc.2024.08.003
- [14] Reid, S., Andrews, J., Christopher, L., and Sarah, T., "Can 3D-Printed Catalysts Improve Hydrogen Peroxide Thruster Performance? An Experimental and Numerical Study," *Chemical Engineering Science*, Vol. 302, 2025, Paper 120783. https://doi.org/10.1016/j.ces.2024.120783
- [15] Baek, S., Jung, W., Kang, H., and Kwon, S., "Development of High-Performance Green-Monopropellant Thruster with Hydrogen Peroxide and Ethanol," *Journal of Propulsion and Power*, Vol. 34, No. 5, 2018, pp. 1256–1261. https://doi.org/10.2514/1.B37081
- [16] Kang, H., Kim, J. W., Lee, J. R., and Kwon, S., "A Mixture of Hydrogen Peroxide and Tetraglyme as a Green Energetic Monopropellant," *Combustion and Flame*, Vol. 210, Dec. 2019, pp. 43–53. https://doi.org/10.1016/j.combustflame.2019.08.016
- [17] Kim, J. W., Bhosale, V. K., Kim, K. S., Lee, S., and Kwon, S., "Room-Temperature Catalytically Reactive Ammonium Dinitramide-H2O2 Monopropellant for Microsatellites," *Advances in Space Research*, Vol. 69, No. 3, Feb. 2022, pp. 1631–1644. https://doi.org/10.1016/j.asr.2021.11.022
- [18] Kim, J. W., Baek, S., Jung, Y., Yoon, W., Ban, H. S., and Kwon, S., "An Alternative ADN Based Monopropellant Mixed with Tetraglyme," *Acta Astronautica*, Vol. 178, Jan. 2021, pp. 241–249. https://doi.org/10.1016/j.actaastro.2020.09.007
- [19] Sutton, G. P., and Biblarz, O., Rocket Propulsion Elements, 9th ed., Wiley, Hoboken, NJ, 2016.
- [20] Hou, Y., Yu, Y., Liu, X., Chen, J., and Zhang, T., "Experimental Study on Microwave-Assisted Ignition and Combustion Characteristics of ADN-Based Liquid Propellant," ACS Omega, Vol. 6, No. 35, Aug. 2021, pp. 22,937–22,944. https://doi.org/10.1021/acsomega.1c03591
- [21] Hou, Y., Yu, Y., Li, Y., Liu, X., Yao, Z., and Zhang, S., "Experimental Study on Microwave Ignition of ADN-Based Liquid Propellant Droplets Doped with Alumina Nanoparticles," *Journal of Physics D: Applied Physics*, Vol. 57, No. 14, Jan. 2024, Paper 145505.
 - https://doi.org/10.1088/1361-6463/ad1b2f
- [22] Wada, A., and Habu, H., "Electric Ignition Characteristics of an Ammonium-Dinitramide-Based Ionic Liquid Monopropellant with Discharge Plasma," AIAA Scitech 2020 Forum, AIAA Paper 2020-1895, Jan. 2020. https://doi.org/10.2514/6.2020-1895
- [23] Tang, Y., Li, S., Yao, Z., Huang, B., and Li, S., "Ignition of an Ionic Liquid Dual-Mode Monopropellant Using a Microwave Plasma Torch," *Proceedings of the Combustion Institute*, Vol. 39, No. 4, 2023, pp. 5063–5071. https://doi.org/10.1016/j.proci.2022.09.003
- [24] Thrasher, J., Williams, S., Takahashi, P., and Sousa, J., "Pulsed Plasma Thruster Development Using a Novel HAN-Based Green Electric Monopropellant," 52nd AIAA/SAE/ASEE Joint Propulsion Conference, AIAA Paper 2016-4846, 2016. https://doi.org/10.2514/6.2016-4846
- [25] Wada, A., Watanabe, H., and Takegahara, H., "Performance Evaluation of a Hydroxylammonium-Nitrate-Based Monopropellant Thruster with Discharge Plasma System," 53rd AIAA/SAE/ASEE Joint Propulsion Conference, AIAA Paper 2017-4757, 2017. https://doi.org/10.2514/6.2017-4757
- [26] Kakami, A., Yamamoto, N., Ideta, K., and Tachibana, T., "Design and Experiments of a HAN-Based Monopropellant Thruster Using Arc-Discharge Assisted Combustion, Transactions of the Japan Society for Aeronautical and Space Sciences," *Aerospace Technology Japan*, Vol. 10, 2012, pp. 13–17. https://doi.org/10.2322/tastj.10.Pa_13
- [27] Kang, H., Lee, J., Kim, K. T., Song, Y. H., and Lee, D. H., "Conceptual Demonstration of Martian Atmosphere-Breathing Electrical Supersonic Thruster with CO2-Based Rotating Gliding Arc," Acta Astronautica, Vol. 200, Nov. 2022, pp. 196–200. https://doi.org/10.1016/j.actaastro.2022.07.058
- [28] An, S., Lee, J., Brahmi, R., Kappenstein, C., and Kwon, S., "Comparison of Catalyst Support Between Monolith and Pellet in Hydrogen Peroxide Thrusters," *Journal of Propulsion and Power*, Vol. 26, No. 3, 2010, pp. 439–445. https://doi.org/10.2514/1.46075

- [29] Tian, H., Zhang, T., Sun, X., Liang, D., and Lin, L., "Performance and Deactivation of Ir/γ-Al₂O₃ Catalyst in the Hydrogen Peroxide Monopropellant Thruster," *Applied Catalysis A: General*, Vol. 210, Nos. 1 and 2, 2001, pp. 55–62. https://doi.org/10.1016/S0926-860X(00)00829-2
- [30] Lee, J., and Kwon, S., "Evaluation of Ethanol-Blended Hydrogen Peroxide Monopropellant on a 10 N Class Thruster," *Journal of Propulsion and Power*, Vol. 29, No. 5, 2013, pp. 1164–1170. https://doi.org/10.2514/1.B34790
- [31] Kang, S., Lee, D., and Kwon, S., "Lanthanum Doping for Longevity of Alumina Catalyst Bed in Hydrogen Peroxide Thruster," *Aerospace Science and Technology*, Vol. 46, 2015, pp. 197–203. https://doi.org/10.1016/j.ast.2015.07.003
- [32] Plumlee, D., Steciak, J., and Moll, A., "Development and Simulation of an Embedded Hydrogen Peroxide Catalyst Chamber in Low-Temperature Co-Fired Ceramics," *International Journal of Applied Ceramic Technology*, Vol. 4, No. 5, 2007, pp. 406–414. https://doi.org/10.1111/j.1744-7402.2007.02161.x
- [33] An, S., and Kwon, S., "Scaling and Evaluation of Pt/Al2O3 Catalytic Reactor for Hydrogen Peroxide Monopropellant Thruster," *Journal of Propulsion and Power*, Vol. 25, No. 5, 2009, pp. 1041–1045. https://doi.org/10.2514/1.40822

- [34] Lee, J., Kim, S., Ryoo, J., Kang, H., and Lee, A., "Conceptual Demonstration of a Modular Fabrication Method for an Engineering Model of a Small Monopropellant Thrusters," *Acta Astronautica*, Vol. 219, June 2024, pp. 506–516. https://doi.org/10.1016/j.actaastro.2024.03.039
- [35] Lee, J., Kim, S., Song, Y., Lee, S., Kang, H., and Lee, A., "Lab-on-PCB Technology for Liquid Monopropellant Microthrusters: Design, Fabrication, and Performance Evaluation," *Sensors and Actuators A: Physical*, Vol. 372, 2024, Paper 115347. https://doi.org/10.1016/j.sna.2024.115347
- [36] Jang, D., Kang, S., and Kwon, S., "Preheating Characteristics of H2O2 Monopropellant Thruster Using Manganese Oxide Catalyst," *Aerospace Science and Technology*, Vol. 41, 2015, pp. 24–27. https://doi.org/10.1016/j.ast.2014.12.010
- [37] Huang, D. H., and Huzel, D. K., Modern Engineering for Design of Liquid-Propellant Rocket Engines, AIAA, Washington, D.C., 1992, pp. 1413–1417. https://doi.org/10.2514/4.866197

V. Sankaran Associate Editor